J. Biochem. **134**, 699–709 (2003)
DOI: 10.1093/jb/mvg195

Induction of PYPAF1 during *In Vitro* Maturation of Mouse Mast Cells

Rei Kikuchi-Yanoshita[1], Yoshitaka Taketomi[1], Kumiko Koga[1], Toshihiko Sugiki[1], Yohei Atsumi[1], Takanori Saito[1], Shin-ichi Ishii[2], Masato Hisada[2], Tamiko Suzuki-Nishimura[2], Masaatsu K. Uchida[2], Tae-Chul Moon[3], Hyeun-Wook Chang[3], Masatsugu Sawada[4], Naoki Inagaki[4], Hiroichi Nagai[4], Makoto Murakami[*,1] and Ichiro Kudo[1]

[1]Department of Health Chemistry, School of Pharmaceutical Sciences, Showa University, 1-5-8 Hatanodai, Shinagawa-ku, Tokyo 142-8555; [2]Department of Pharmacology, Meiji Pharmaceutical University, 2-522-1 Nishio, Kiyose, Tokyo 204-8588; [3]College of Pharmacy, Yeungnam University, Gyonsan, Korea; and [4]Pharmacological Department, Gifu College of Pharmacy, 5-6-1 Mitahora Higashi, Gifu 502-8585

Received August 14, 2003; accepted September 4, 2003

Coculture of mouse bone marrow-derived immature mast cells (BMMC) with Swiss 3T3 fibroblasts in the presence of stem cell factor (SCF) promotes morphological and functional maturation toward a connective tissue mast cell (CTMC)–like phenotype, which is accompanied by increased expression of several unique genes. Here we report the molecular identification of one of them, mast cell maturation–associated inducible gene (MMIG)-1. The MMIG-1 cDNA encodes a 117-kDa cytosolic protein that comprises an N-terminal PYRIN domain, a central nucleotide-binding domain, and nine C-terminal leucine-rich repeats. MMIG-1 shows >85% sequence similarity to human cryopyrin/PYPAF1, a causal gene for familial cold urticaria and Muckle-Wells syndrome. MMIG-1 was distributed in the cytosol of CTMC-like differentiated BMMC. MMIG-1 underwent alternative splicing in the leucine-rich repeats and each variant was induced differently in BMMC during coculture. Moreover, its expression was increased in the ears of mice with experimental atopic dermatitis. Thus, MMIG-1, a likely mouse PYPAF1 ortholog, may play a role in mast cell–directed inflammatory diseases.

Key words: allergy, differentiation, inflammation, mast cell, mouse.

Abbreviations: BMMC, bone marrow-derived mast cells; CTMC, connective tissue mast cells; MMC, mucosal mast cells; MMIG, mast cell maturation inducible gene; SCF, stem cell factor, FcεRI, high affinity receptor for IgE; IL, interleukin; NBS, nucleotide-binding site; LRR, leucine-rich repeat; DNFB, dinitrofluorobenzene; CARD, caspase recruitment domain; PBS, phosphate-buffered saline; TBS, Tris-buffered saline; SDS-PAGE, sodium dodecyl sulfate–polyacrylamide gel electrophoresis.

Mast cells express high-affinity receptor for IgE (FcεRI) on their surface and are activated to secrete a variety of potently biologically active mediators in response to challenge with multivalent antigens (*1*, *2*). The release of such mediators from mast cells represents a critical component of many clinically important allergic reactions, various chronic inflammatory diseases and innate immunity (*3*, *4*). Mast cells in different anatomical microenvironments show variation in multiple aspects of their phenotypes and their sensitivity to various agents that can influence their functions (*1*, *2*). The growth and development of mast cells are regulated by the tissue-derived cytokine stem cell factor (SCF), a ligand for the Kit receptor tyrosine kinase (*1*, *2*).

Rodent mast cells are subdivided into connective tissue mast cells (CTMC) and mucosal mast cells (MMC), changing their phenotypes rapidly depending on the current microenvironments in which they reside (*5*, *6*). CTMC exhibit several remarkable features that are not shown by MMC or interleukin (IL)-3–dependent mouse bone marrow-derived mast cells (BMMC), which represent an *in vitro* culture-derived, relatively immature population of mast cells (*1*, *2*). BMMC can differentiate into CTMC-like cells *in vitro* after coculture with fibroblasts in the presence of appropriate mast cell-poietic cytokines (*7–10*). For instance, we recently reported that the coculture of BMMC with 3T3 fibroblasts in the presence of recombinant SCF changes their morphological and functional properties from an immature to mature CTMC-like phenotype within only 2–4 days (*10*).

In an effort to determine comprehensively the profiles of expressed genes in immature and mature mast cells, we have performed cDNA subtraction between BMMC before and after such coculture to identify genes that are upregulated during the mast cell maturation process (*11*). Amongst a number of unique inducible genes identified so far by means of this approach, we have designated seven unknown genes as mast cell maturation-associated inducible genes (MMIGs). In this study, we report the complete structure of MMIG-1, which shows the highest sequence homology with human cryopyrin/PYPAF1, a very recently identified molecule belonging to the PYRIN domain-containing signal transducer family (*12*, *13*).

MATERIALS AND METHODS

Cell Culture and Activation—The culture of BALB/c mouse-derived BMMC, rat mastocytoma RBL-2H3 cells

*To whom correspondence should be addressed. Tel: +81-3-3784-8196, Fax: +81-3-3784-8245, E-mail: mako@pharm.showa-u.ac.jp

and mouse leukemia WEHI-3B cells, and activation of mast cells with IgE and antigen were described previously (*11*).

Coculture of BMMC with Swiss 3T3 Fibroblasts—The procedure for coculture of BMMC and Swiss 3T3 fibroblasts in the presence of SCF was described previously (*10*). Briefly, BMMC were washed once, suspended at 2×10^5 cells/ml in enriched medium supplemented with 100 ng/ml SCF, and seeded on confluent Swiss 3T3 fibroblast monolayers grown in 24-well plates (1 ml/well), 12-well plates (2 ml/well), 35-mm diameter dishes (3 ml/dish), and 100-mm dishes (10 ml/dish) (Iwaki Glass, Tokyo), as required for the experiments. The medium was changed every 2 days. Mast cells largely attached to the fibroblast monolayer during the coculture. After appropriate periods of coculture (for up to 6 days), the cells (a mixture of mast cells and fibroblasts) were trypsinized, resuspended in enriched medium, and then re-seeded into T75 flasks. After 30-min incubation, most fibroblasts attached to the bottom of the flasks, and >95% of the floating cells were mast cells, as determined from their morphology and on alcian blue/safranin staining (*10*). These floating cells were used as the cocultured BMMC. The viability of BMMC was maintained at nearly 100% under these culture conditions.

PCR-Selected cDNA Subtraction—The procedure for cDNA subtraction, by which a set of inducible genes in BMMC during the coculture were enriched, was conducted with a PCR-selected™ cDNA subtraction kit (Clontech, Palo Alto, CA), as described previously (*11*). The cDNA inserts were subjected to RNA blotting to confirm their induction in BMMC and their absence in Swiss 3T3 after coculture.

Cloning of MMIG-1 cDNA—A cDNA library was prepared from poly(A)$^+$ RNA of cocultured BMMC using a Super Script™ Lamda System for cDNA Synthesis and Cloning Reagent Assembly (Invitrogen, San Diego, CA) and λ-Zip LOX *Not*I/*Sal*I Arms (Invitrogen), according to the manufacturer's instructions. Approximately 75,000 clones were screened with the MMIG-1 fragment, which was originally obtained on the cDNA subtraction as noted above, as a probe. A positive phage clone (*4C2*) was transformed into *E. coli* DH12S(ZIP) (Invitrogen), in which it was excised into a plasmid form (pZL1). Poly(A)$^+$ RNA was prepared from 10^8 BMMC after coculture with a Fast Track™ 2.0 mRNA isolation kit (Invitrogen). After the phosphate group was removed from the 5′-ends of uncapped poly(A)$^+$ RNAs using A19 bacterial alkaline phosphatase (Takara Biomedicals, Ohtsu), the cap structure, 7-methylated-GTP, of intact capped poly(A)$^+$ RNAs was replaced with a phosphate residue by treatment with tobacco acid pyrophosphatase (Nippon Gene, Toyama). The decapped poly (A)$^+$ RNA was then ligated with an oligoribonucleotide, 5′-rGrArGrArGrCrArArGrGUrA rCrGrCrCrArCrArGrCrGUrAUrGrAUrGrC-3′ (Genset Oligos, Kyoto), using T4 RNA ligase (Takara Biomedicals). The oligo-capped poly(A)$^+$ RNA thus prepared was transcribed into cDNA using SuperScript II reverse transcriptase (Invitrogen). The 5′-end sequence of the MMIG-1 cDNA was amplified with *ex*Taq polymerase (Takara Biomedicals) using the cDNA obtained by the oligo-capping method as a template with a set of primers, 5′-CAAGGTACGCCACAGCGTATG-3′, a sequence within the synthetic oligoribonucleotide used, and 5′-AGCGGAGAC GTCAGCCTT CTG-3′, a sequence within the 1,890-bp fragment that was obtained by RT-PCR (see "RESULTS") under the following conditions: 5 min at 94°C, followed by 35 cycles of 30 s at 94°C, 30 s at 60°C, and 3 min at 72°C. The amplified product was subcloned into the pCR4 vector (Invitrogen). The sequences of the cDNA inserts were determined with a Thermo Sequenase fluorescent-labelled primer cycle sequencing kit with 7-deaza-dGTP (Amersham Bioscience, Piscataway, NJ) using a DNA sequencer DSQ-1000L (Shimadzu, Kyoto).

To determine the genomic organization of the MMIG-1 gene, a mouse genomic library of adult BALB/c mouse liver (Clontech, Palo Altp, CA) was screened with clone 4C2 by the standard plaque hybridization method. Positive clones were treated with NotI or EcoRI (Takara Biomedicals), and the digested inserts were subcloned into the pCR3.1 vector (Invitrogen) and sequenced. Alternatively, the nucleic acid database was searched using the BLASTn system with MMIG-1 cDNA as a reference.

Preparation of FLAG-Tagged MMIG-1—The full-size MMIG-1 cDNA with a FLAG-tag at the C-terminus was amplified from cocultured BMMC poly(A)$^+$ RNA by RT-PCR with a pair of primers, 5′-ATGACGAGTGTCTGCAAGCTGGC-3′ and 5′-TCACTTGTCATCGTCGTCCTTGTAGTCCCAGGAAATCTCGAAGAC-3′ (FLAG epitope underlined), which were designed based on the sequences of the 5′- and 3′-ends of the open reading frame. The amplified product was subcloned into mammalian expression vector pcDNA3.1/V5/His TOPO (Invitrogen) and sequenced as described above.

Transfection Experiments—To obtain HEK293 cells stably overexpressing MMIG-1-FLAG, 1 μg of MMIG1-FLAG in the pcDNA3.1/V5/His TOPO expression vector was mixed with 2 μl of Lipofectamine PLUS (Invitrogen) in 100 μl of Opti-MEM medium (Invitrogen) for 30 min and then added to cells that had attained 40–60% confluence in 12-well plates (Iwaki Glass) containing 0.5 ml of Opti-MEM. Two days after the transfection, the cells were cloned by limiting dilution in 96-well plates in culture medium supplemented with 1 mg/ml geneticin (Invitrogen). After culture for 3–4 weeks, wells containing a single colony were chosen, and protein expression was assessed by Western blotting using anti-FLAG monoclonal antibody M2 (Sigma, St. Louis, MI).

Preparation of Anti-MMIG-1 Antibody—cDNAs for the full-length MMIG-1 and its truncated form (residues 91–216, which corresponds to the linker region between the PYRIN and NBS domains; see "RESULTS"), were subcloned into the pET-21c vector (Novagen) at the EcoRI site and then transformed into *E. coli* (BL21(DE3); Invitrogen). After culture with 0.4 mM isopropyl-thio-β-D-galactoside, the produced recombinant His_6-tagged truncated MMIG-1 protein was purified from bacterial homogenates with a Ni-NTA column (QIAGEN) to near homogeneity according to the manufacturer's instruction and then dialyzed against TBS. The purified protein gave a single band corresponding to the predicted size on sodium dodecyl sulfate-polyacrylamide gel electrophoresis (SDS-PAGE) followed by staining with Coomassie brilliant blue.

New Zealand White rabbits (male, 1 kg; Saitama Animal Center) were immunized subcutaneously with the

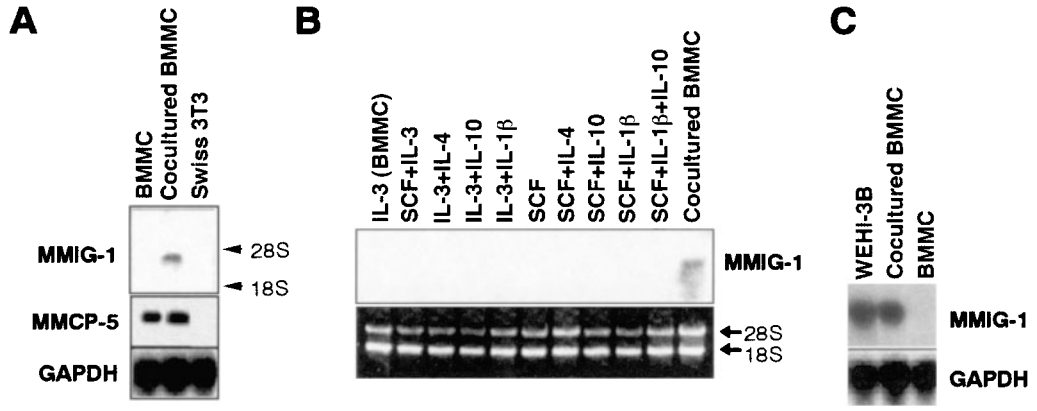

Fig. 1. **Induction of MMIG-1 in BMMC after coculture with Swiss 3T3 in the rpesence of SCF.** (A) Expression of MMIG-1 and mouse mast cell protease-5 (MMCP-5) mRNAs in BMMC before and after coculture with Swiss 3T3 cells in the presence of SCF for 4 days. MMIG-1 was undetectable in Swiss 3T3 cells used for coculture. (B) Expression of MMIG-1 mRNA in BMMC cultured for 4 days in the presence of various combinations of cytokines and in BMMC cocultured with Swiss 3T3 in the presence of SCF. (C) Expression of MMIG-1 mRNA in WEHI-3B cells. The results were evaluated by Northern blotting (A and C) and RT-PCR (B). Appropriate sample loading into each lane was verified by visualizing ribosomal RNA in agarose gels with ethidium bromide (B) or by Northern blotting of glyceraldehyde-3-phosphate dehydrogenase (GAPDH) (A and C).

purified truncated MMIG-1 protein (0.1 mg each) mixed with Freund's complete adjuvant (Difco). After several booster immunizations with Freund's incomplete adjuvant (Difco) at 2-wk intervals, blood was collected and the serum titer was determined by means of enzyme-linked immunosorbent assay and Western blotting with the recombinant full-length MMIG-1 protein expressed in *E. coli*, as described above. The specific binding of the antibody to MMIG-1 was verified by immunoblotting using cell lines expressing MMIG-1 (see "RESULTS").

Western Blotting—Samples were subjected to SDS-PAGE on 7.5% (w/v) gels under reducing condition. The separated proteins were electroblotted onto nitrocellulose membranes (Schleicher and Schuell, Dassel, Germany) using a semi-dry blotter (Bio-Rad, Hercules, CA). After blocking with 3% skim milk in 10 mM Tris-HCl (pH 7.4) containing 150 mM NaCl (TBS), the membranes were sequentially incubated with an anti-FLAG antibody (1: 20,000 dilution in TBS containing 0.05% Tween-20) or anti-MMIG-1 antibody (1:5,000 dilution) for 2 h and horseradish peroxidase-conjugated anti-mouse IgG (Amersham Bioscience) (1:5,000 dilution in TBS containing 0.05% Tween-20) for 1 h, and then visualized using an ECL system (NEN™ Life Science Products, Boston, MA).

Northern Blotting—Total RNA was purified from the cells using TRIZOL reagent (Invitrogen). Approximately 10 μg of total RNA was applied to each lane of 1.2% (w/v) formaldehyde-agarose gels, followed by electrophoresis and then transfer to Immobilon-N membranes (Millipore, Bedford, MA). The resulting blots were then sequentially probed with the MMIG-1 cDNA fragment that had been labeled with [^{32}P]dCTP (NEN™ Life Science Products) by random priming (Takara Biomedicals). All hybridizations were carried out at 42°C overnight in a solution comprising 50% (v/v) formamide, 0.75 M NaCl, 75 mM sodium citrate, 0.1% (w/v) SDS, 1 mM EDTA, 10 mM sodium phosphate, pH 6.8, 5× Denhardt's solution (Nacalai Tesque, Tokyo), 10% (w/v) dextran sulfate (Sigma), and 100 μg/ml salmon sperm DNA (Sigma). The blots were visualized by autoradigraphy with Kodak X-OMAT AR films and double intensifying screens at –80°C.

Confocal Laser Microscopy—Cells grown on collagen-coated cover glasses (Iwaki Glass) were fixed in 10% (v/v) formalin in phosphate-buffered saline (PBS) for 30 min and then permeabilized with 0.2% (v/v) Triton X-100 in PBS for 2 min. Then the cells were sequentially treated with 3% (v/v) BSA in PBS for 2 h, the anti-FLAG antibody (1:500 dilution) or anti-MMIG-1 antibody (1:100 dilution) in 1% bovine serum albumin (BSA) in PBS for 2 h, and FITC-conjugated second antibody (1:100 dilution) (Zymed, South San Francisco, CA) in 1% BSA in PBS for 1 h, with 3 washes with PBS in each interval. After 6 washes with PBS, the cells were mounted on glass slides and the fluorescent signal was visualized under a laser scanning confocal microscope (IX70; Olympus, Tokyo).

Experimental Atopic Dermatitis—Five repeated topical applications of 2,4-dinitrofluorobenzene (DNFB) to the ears of BALB/c, but not C57BL/6, mice result in contact hypersensitivity of the ears and significant elevation of the serum IgE level, accompanied by an increased T_{H1} response on the onset of skin dermatitis and a T_{H2} response in the lymph nodes (*14*). Briefly, mouse ears were painted with 25 μl of 0.15% (w/v) DNFB or vehicle (acetone:olive oil, 3:1) once a week. The ears were removed 4 h after the fifth painting and subjected to RNA extraction. Replicate ear sections were fixed with formalin, embedded in paraffin, and then stained with hematoxylin and eosin to verify the progress of inflammation.

RESULTS

Expression of MMIG-1 in Mast Cells—Fig. 1 depicts the induction of MMIG-1 during *in vitro* maturation of mouse BMMC toward a CTMC phenotype. As assessed by RNA blotting, induction of MMIG-1 occurred when BMMC were cocultured with Swiss 3T3 cells in the presence of SCF, whereas expression of mouse mast cell protease-5 was unchanged during such coculture (Fig. 1A). None of the mast cell–poietic cytokines tested alone or in

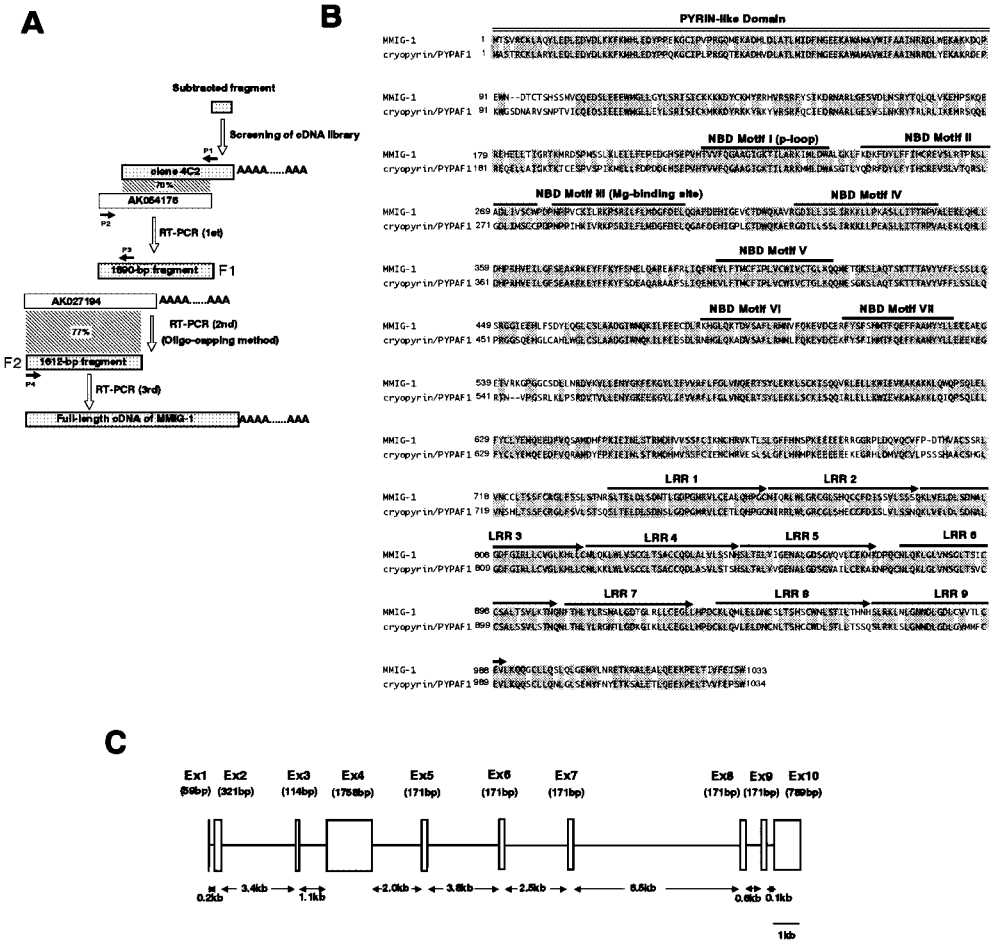

Fig. 2. **Cloning of MMIG-1.** (A) Full-length MMIG-1 cDNA was cloned from poly(A)$^+$ RNA of cocultured BMMC through four steps from the original fragment obtained on cDNA subtraction. Clone 4C2 was obtained by screening of a cocultured BMMC cDNA library using the subtracted fragment as described under "MATERIALS AND METHODS." The 1,890-bp F1 fragment was obtained by RT-PCR (1st) with a set of primers, P1 (5′-CTA CCAG-GAAATCTCGAAGACTA-3′) and P2 (5′-ATGTGCTTCATCCCCCT-GGTC TGT-3′). The 1,612-bp F2 fragment was amplified from oligo-capped poly(A)$^+$ RNA prepared by the oligo-capping method (2nd RT-PCR), using 5′-CAAGGTACG-CC ACAGCGTATG-3′, a sequence within the oligoribonucleotide, and P3 (5′-AGCGGAGACGTCA-GTCTT CTG-3′). The open reading frame of MMIG-1 with a 5′-noncoding sequence was amplified by RT-PCR (3rd) using a set of primers, P1 and P4 (5′-ACCC-AAGGCTGCTATCTGG-3′). The full-length cDNA was obtained by connecting the open reading frame with the 3′-nonconding sequence found in clone 4C2. The percentages in the shadowed boxes represent the similarities in nucleotide sequence between clone 4C2 and AK054176 and between the F2 and AK027194. Bold arrows indicate the positions of the primers used for the RT-PCR. (B) Amino acid sequence alignment of MMIG-1 and human cryopyrin/PYPAF1. MMIG-1 has a PYRIN domain, an NBS domain consisting of 7 motifs (I–VII), and 9 LRRs. Alignment was performed with the Clustal W mutiple alignment program. Amino acids conserved in both proteins are shadowed. (C) Genomic organization of the mouse *MMIG-1* gene. The *MMIG-1* gene consists of at least 10 exons spanning over 24 kbp, and is located on mouse chromosome 11.

combination, including SCF, IL-3, IL-4, IL-10, and IL-1β, induced MMIG-1 expression (Fig. 1B), implying that MMIG-1 expression in BMMC requires a specific condition for maturation toward a CTMC-like phenotype. Since MMIG-1 was undetectable in Swiss 3T3 even after coculture (Fig. 1A), it is unlikely that the increased expression of MMIG-1 after coculture was due to minor contamination by Swiss 3T3 cells of the mast cell preparations. Of several cell lines tested, WEHI-3B, a mouse T-cell leukemia cell line, expressed comparable MMIG-1 to cocultured BMMC (Fig. 1C), whereas its expression was barely detectable in various fibroblastic, epithelial, and neuronal cell lines (data not shown).

Cloning of MMIG-1—A cDNA library of cocultured BMMC was prepared and screened by means of plaque hybridization using a 126-bp MMIG-1 fragment obtained from the cDNA subtraction as a probe (the scheme is illustrated in Fig. 2A). A positive clone with a 2,120-bp fragment, termed clone 4C2, was obtained that contained a poly(A)$^+$ tail. The fragment originally obtained on cDNA subtraction corresponded to a region near the 3′ end of 4C2 (Fig. 2A). Although 4C2 showed 70% homology with EST gene AF054176, it did not contain a region corresponding to the 5′-end of AF054176. Therefore, we performed RT-PCR from poly(A)$^+$ RNA of cocultured BMMC using a sense primer designed based on the 5′-end of AF054176 and an antisense primer corresponding to a region in 4C2 that shows the highest homology with AF054176 (Fig. 2A). A 1,890-bp fragment (F1) with the expected overlapping sequence with 4C2 was obtained. The amino acid sequence predicted from this fragment exhibited 84% similarity to AF054176, whereas the C-terminal region was less homologous (43%) (Fig. 2A). We then found another EST gene, AK027194, in the database, the 3′-region of which was identical to the 5′-region of AF054176. Therefore, it appeared that the F1 fragment still lacked the 5′-end of the full-length MMIG-1 cDNA. We then used the oligo-capping method, where the cap structure of the intact capped poly(A)$^+$ RNA from cocultured BMMC was replaced with a synthetic oligoribonucleotide, and then RT-PCR was carried out with a pair of primers directed to the sequences of the synthetic oligoribonucleotide and the F1 fragment (a region about 280-bp downstream from the 5′-end; see Fig. 2A). A novel 1,612-bp fragment (F2) was obtained that showed 77% homology with AK027194 and contained the expected overlapping region of ~280 bp as well as the starting ATG codon (Fig. 2A). The full-length MMIG-1 cDNA contain-

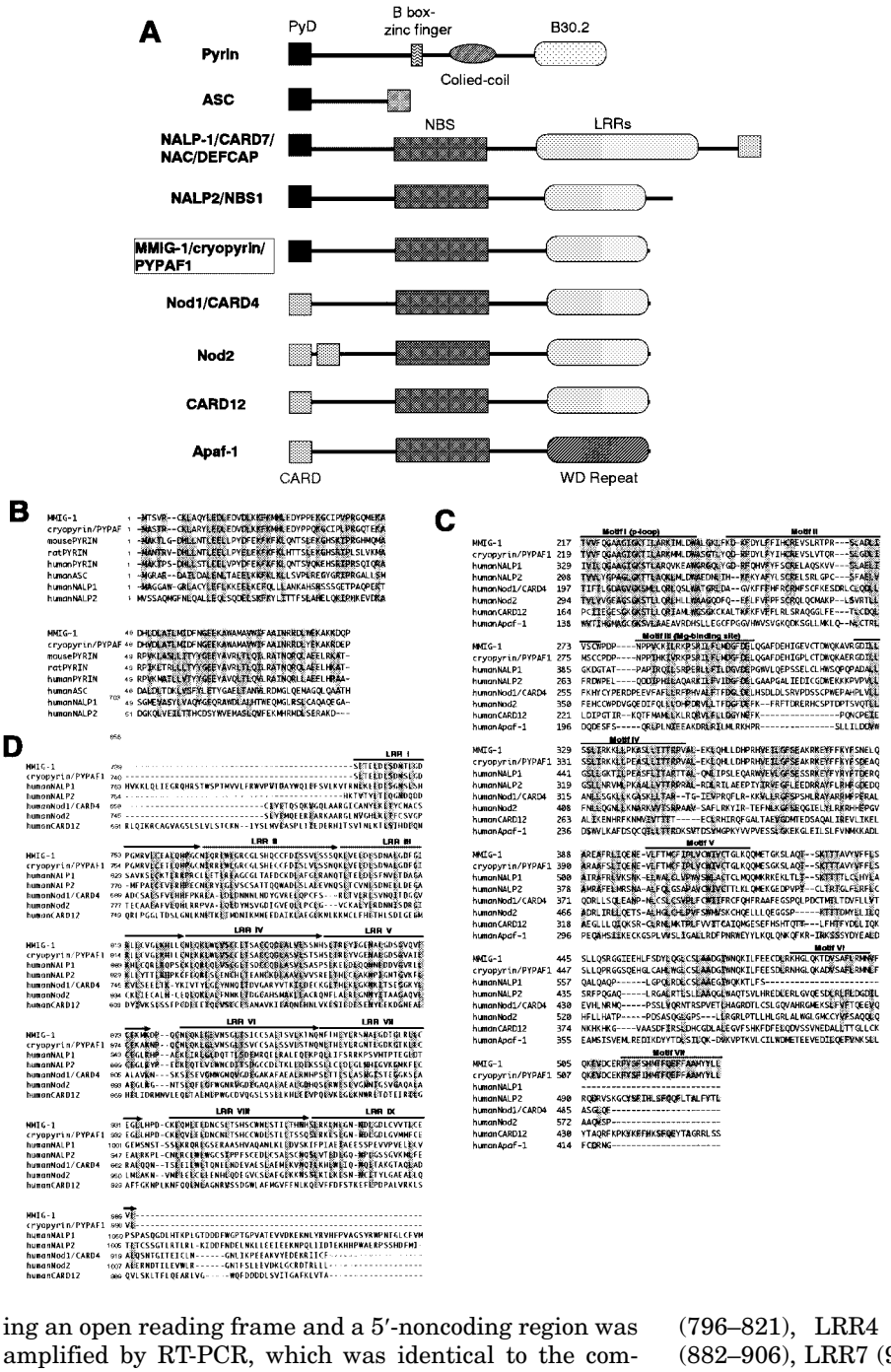

Fig. 3. **Structural features of MMIG-1 and related proteins.** (A) Domain structures of MMIG-1 and related proteins, which have PYRIN, NBS and/or LRR domains. Amino acid alignment of the PYRIN (B), NBS (C), and LRR (D) domains among these proteins is shown. Alignment was performed with the Clustal W mutiple alignment program. Identical or similar amino acid residues are shadowed.

ing an open reading frame and a 5′-noncoding region was amplified by RT-PCR, which was identical to the combined sequences of 4C2, F1, and F2.

The open reading frame of MMIG-1 cDNA (GenBank accession number AF486632) is 3,202 bp in length (nucleotides 123–3224), and encodes a protein that consists of 1,033 amino acids (Fig. 2B). As illustrated in Fig. 2B, the MMIG-1 protein has a PYRIN-like domain in the N-terminal region (residues 1–90), a nucleotide-binding site (NBS) domain (or NACHT domain) (residues 217–532), in which there are 7 consensus motifs, namely I (P-loop; residues 217–239), II (246–276), III (Mg^{2+}-binding site; 280–303), IV (324–349), V (400–420), VI (487–502), and VII (513–532), in the central region, and 9 leucine-rich repeats (LRRs) in the C-terminal region [residues 739–966; LRR1 (residues 739–766), LRR2 (768–795), LRR3 (796–821), LRR4 (826–848), LRR5 (853–877), LRR6 (882–906), LRR7 (911–925), LRR8 (930–966), and LRR9 (967–990)]. Thus, MMIG-1 is a member of the PYRIN domain–containing protein family that also possesses a NBS domain and LRRs. The organization of the *MMIG-1* gene, as determined on mouse liver genomic library screening and the database search, is shown in Fig. 2C. The *MMIG-1* gene consists of at least 10 exons spanning more than 24 kbp, and is located on mouse chromosome 11. The starting ATG is located in exon 2 and the terminating TGA in exon 10.

Proteins related to MMIG-1 in terms of domain structures are illustrated in Fig. 3A. The PYRIN domain of MMIG-1 exhibits significant homology with those of other PYRIN-containing proteins, such as pyrin (*15*, *16*), DEFCAP-L (CARD7/NAC/NALP-1) (*17*, *18*), NALP-2

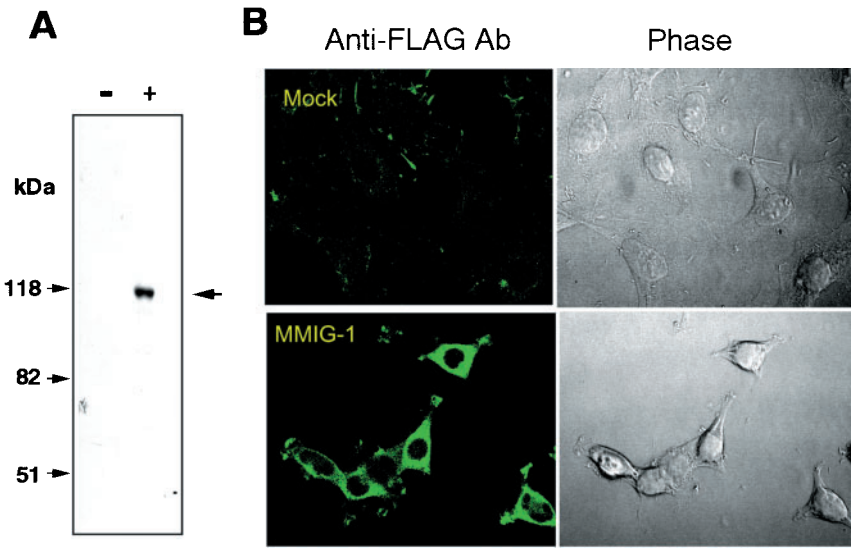

Fig. 4. **Expression of MMIG-1 protein.** (A) Expression of MMIG-1 protein in HEK293 transfectants. Sonicates of cells stably transfected with C-terminally FLAG-tagged MMIG-1 (+) or the empty vector (–) were subjected to Western blotting with an anti-FLAG antibody. (B) Immnofluorescence confocal microscopy of HEK293 transfectants with the anti-FLAG antibody. Mock- (top) and MMIG-1-FLAG- (bottom) transfected HEK293 cells were fixed, permeabilized, and immunostained with the anti-FLAG antibody (left). Phase contrast images of cells are also shown (right).

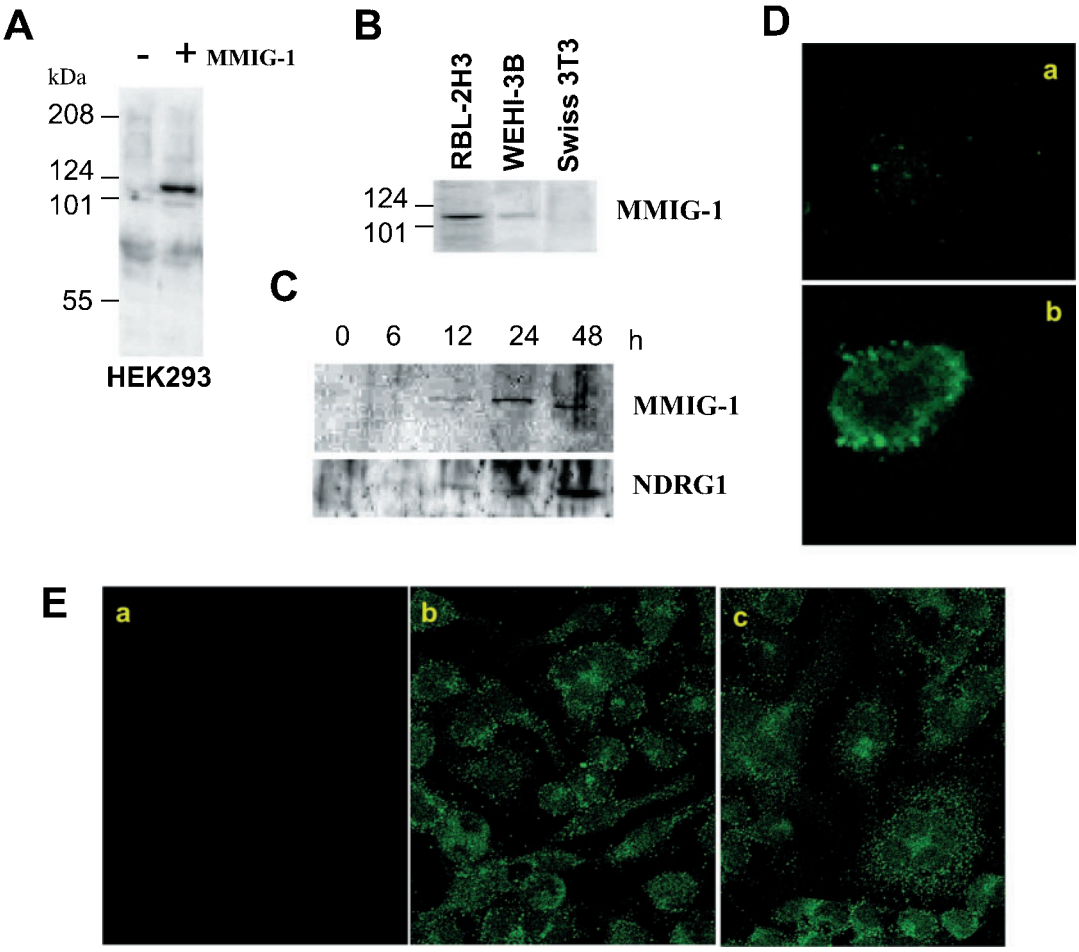

Fig. 5. **Detection of MMIG-1 protein with an anti-MMIG-1 antibody.** (A) Expression of MMIG-1 protein in HEK293 transfectants. Sonicates of cells stably transfected with C-terminally FLAG-tagged MMIG-1 (+) or the empty vector (–) were subjected to Western blotting with an anti-MMIG-1 antibody. (B) Detection of endogenous MMIG-1 protein in several cell lines. (C) Time course of MMIG-1 and NDRG1 protein induction in BMMC during coculture with Swiss 3T3 cells in the presence of SCF. (D) Immunocytostaining of endogenous MMIG-1 protein in BMMC. BMMC before (a) and after (b) coculture for 2 days were fixed, permeabilized, and then immunostained with the anti–MMIG-1 antibody. Magnification, ×100. (E) Immunocytostaining of endogenous MMIG-1 protein in RBL-2H3 cells. Cells before (a, b) and after (c) stimulation for 10 min with IgE and antigen were subjected to staining with (b, c) or without (a) the anti-MMIG-1 antibody. Magnification, ×40.

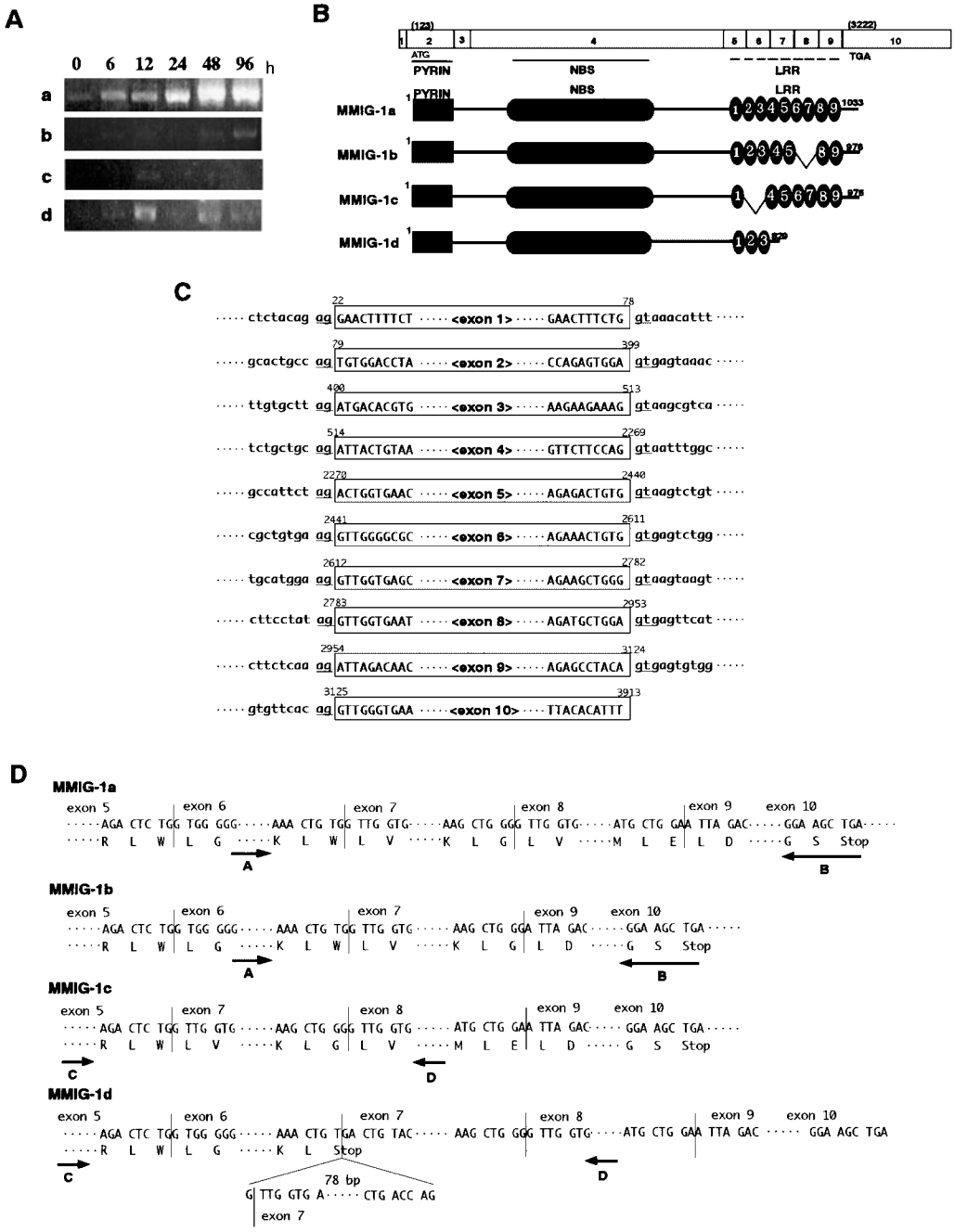

Fig. 6. **Identification of spliced variants of MMIG-1.** (A) RT-PCR amplification of the C-terminal region of MMIG-1 from BMMC cocultured with Swiss 3T3 in the presence of SCF for the indicated periods. In addition to the band corresponding to the full-length MMIG-1a (indicated as "a" on the right side), three shorter bands corresponding to MMIG-1b, MMIG-1c, and MMIG-1d (indicated as "b", "c," and "d") were detected. (B) Structures of MMIG-1 spliced variants. In comparison to the full-size MMIG-1a, MMIG-1b lacks LRR6 and LRR7, MMIG-1c lacks LRR2 and LRR3, and MMIG-1d has only three LRRs (LRR1, 2, and 3). The relationship between the domains and the exons is illustrated at the top. The numbers in parentheses represent the nucleotide numbers of the starting ATG and terminating TGA. (C) Nucleotide sequences of the exon–intron junctions. The sequences of splicing donor and acceptor sites are gt and ag, respectively, in all cases. (D) Nucleotide and amino acid sequences around the splicing sites of the variants. A 78-bp fragment deleted from MMIG-1d is shown at the bottom. Arrows indicate the primers, A–D, used to distinguish the isoforms. The PCR conditions were 5 cycles of 95°C for 30 s and 72°C for 2 min, 5 cycles of 95°C for 30 s and 70°C for 2 min, and 30 cycles of 95°C for 30 s and 68°C for 2 min.

(NBS1) (*19*), and ASC (*20*, *21*) (Fig. 3B). Like MMIG-1, DEFCAP-L and NALP-2 consist of an N-terminal PYRIN domain, a central NBS domain, and C-terminal LRRs (*17–19*). The NBS domain and LRRs of MMIG-1 also show low homology with those of other NBS (Fig. 3C) or LRR (Fig. 3D) proteins such as human Nod1 (CARD4) (*22*), Nod2 (*23*), and CARD12 (*24*), which have an N-terminal caspase recruitment domain (CARD) in place of the PYRIN domain (Fig. 3A). Apaf-1, a central regulator of apoptosis that activates procaspase-9 in the presence

of cytochrome *c* (*25*), also contains a central NBS domain, although the C-terminal LRRs are replaced by WD40 repeats (Fig. 3A). While this manuscript was in preparation, a novel human protein containing these three domains was identified (*12*, *13*). This protein, termed cryopyrin/PYPAF1, shows 82.4% identity with MMIG-1 over the whole amino acid sequence (Fig. 2B). The PYRIN domain, NBS domain and LRRs of cryopyrin/PYPAF1 are 88.9%, 87.3%, and 85.3% identical, respectively, to those of MMIG-1. It is therefore likely that MMIG-1 is a mouse counterpart of PYPAF1 or a closely related molecule.

Subcellular Distribution of MMIG-1—When FLAG-tagged MMIG-1 was transfected into HEK293 cells, a cell line which had been used successfully for transfection with other PYRIN domain or NBS/LRR-containing proteins (*17–25*), the MMIG-1-FLAG protein was expressed as the predicted 117-kDa protein, as seen on immunoblotting using an anti-FLAG antibody (Fig. 4A). Immunocytostaining of this HEK293 clone revealed that the MMIG-1-FLAG protein was localized in the cytosol (Fig. 4B).

To assess the expression of the MMIG-1 protein in mast cells, we prepared an antibody that specifically recognizes MMIG-1. To avoid possible cross-reaction with other proteins bearing homologous domains, we expressed a GST-fused linker region (residues 91–216) between the PYRIN and NBS domains of MMIG-1 in *E. coli*, purified it to near homogeneity on a glutathione-Sepharose column, and then immunized rabbits with it. On immunoblotting, the obtained antiserum recognized a 117-kDa protein in *E. coli* cells transfected with the full-length MMIG-1 cDNA (data not shown) and that in MMIG-1–transfected, but not parent, HEK293 cells (Fig. 5A). Endogenous MMIG-1 protein was detectable in RBL-2H3 cells, a rat mast cell line, and in WEHI-3B cells, but not in Swiss 3T3 cells, on immunoblotting (Fig. 5B). The expression of endogenous MMIG-1 protein was undetectable in BMMC before coculture, became evident at 12 h, and reached a plateau level by 24–48 h of coculture (Fig. 5C). In comparison, the induction of NDRG1, another protein that is markedly induced in BMMC during such coculture (*11*), occurred with a similar time course (Fig. 5C).

Immunocytostaining with this antibody revealed that endogenous MMIG-1 was localized in the cytosol of BMMC after coculture, whereas it was undetectable in BMMC without coculture (Fig. 5D). There were some intensely stained dot-like structures in cocultured BMMC (Fig. 5D, panel b). In RBL-2H3 cells, endogenous MMIG-1 exhibited a punctate distribution throughout the cytosol, which was unaltered after stimulation for 10 min with IgE and antigen (Fig. 5E). The punctate signal observed in cocultured BMMC and RBL-2H3 cells may be a reflection of the PYRIN domain-mediated assembly of MMIG-1 with ASC, which is known to form aggregates called "specks" in the cytosol (*20*, *21*). Indeed, in our preliminary study, ASC mRNA was detected in BMMC and its expression was unchanged during coculture, as assessed by RT-PCR (data not shown).

Alternative Splicing of MMIG-1—When RT-PCR was performed to amplify the C-terminal region of MMIG-1 from cocultured BMMC, several additional fragments that were shorter than the predicted size appeared, even

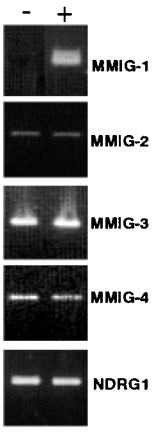

Fig. 7. **Induction of MMIG-1/PYPAF1 in the ears of mice with DNFB-induced atopic dermatitis.** Total RNAs obtained from the ears of BALB/c mice 4 h after the fifth treatment with DNFB (+) or the vehicle (–) were subjected to RT-PCR using specific primers for MMIG-1 as well as for NDRG1 and other MMIGs (MMIG-2–4). The PCR conditions for NDRG1 and MMIG-2, -3, and -4 were given elsewhere (*11*).

though the expression levels of these fragments were much lower than that of the full-size MMIG-1 (Fig. 6A). Sequencing of these shorter fragments revealed that they were truncated in the LRR domain, which apparently arose through alternative splicing (Fig. 6B). We therefore designated the full-length molecule (*i.e.* containing all 10 exons) as MMIG-1a, and the ones lacking exon 8, exon 6 and part of exon 7 as MMIG-1b, MMIG-1c, and MMIG-1d, respectively. MMIG-1b and MMIG-1c each consist of 976 amino acids having 7 LRRs (compared with 9 LRRs in MMIG-1-a), and MMIG-1d consists of 829 amino acids with only 3 LRRs (Fig. 6B).

MMIG-1a, the full-length and predominant form, was poorly expressed in BMMC, started to increase as early as 6 h after the start of coculture, and reached a peak by 48–96 h (Fig. 6A). This was largely in agreement with the change in MMIG-1 protein expression (Fig. 5C). The expression of MMIG-1b was rather weak, being detected at 48–96 h (Fig. 6A). The expression of MMIG-1c was transient, being detected only at 12 h, and MMIG-1d, the shortest isoform with only 3 LRRs, showed biphasic induction, reaching first and second expression peaks at 12 h and 48 h, respectively (Fig. 6A).

The exon–intron junctions of the *MMIG-1* gene are shown in Fig. 6C. In each case, the intron sequence at the 5′-boundary of the exon ends in the dinucleotide AG, and that at the 3′-boundary of the exon begins with the dinucleotide GT, which is consistent with the recognized rule for sequences at such junctions. The sequences around the splicing sites of MMIG-1b, MMIG-1c, and MMIG-1d are shown in Fig. 6D. In the case of MMIG-1d, a 78-bp fragment, which spans from the end of exon 6 to the middle of exon 7, was deleted, resulting in the appearance of the termination codon (Fig. 6D).

Induction of MMIG-1 in Mouse Ear Atopic Dermatitis—Repeated topical application of DNFB to the ears of BALB/c, but not C57BL/6 mice, results in contact hypersensitivity of the ears and significant elevation of the

serum IgE level, accompanied by an increased T_{H1} response on the onset of skin dermatitis and a T_{H2} response in the lymph nodes (*14*). The expression of MMIG-1 in the ears of BALB/c mice after five applications of DNFB was analyzed by RT-PCR. The expression of MMIG-1 was rather higher after the fifth application of DNFB than in vehicle-treated control ears (Fig. 7). In contrast, there were no significant differences in the expression of NDRG1 and other MMIGs [ADP-ribosylation factor–like protein 7, mouse mast cell protease-9 and dual specificity phosphatase 4, which were designated as MMIG-2, -3, and -4 in our previous study (*11*)] between DNFB- and vehicle-treated mice (Fig. 7). Expression levels of MMIG-1, NDRG1 and other MMIGs were not increased in replicate C57BL/6 mice (data not shown), a non-responder strain (*14*). These results suggest that the experimental atopic dermatitis is accompanied by a selective and marked increase in MMIG-1 expression.

DISCUSSION

Of a particular panel of genes that were markedly induced during *in vitro* differentiation and maturation of BMMC toward a CTMC-like cells (*11*), we have deduced the complete cDNA and amino acid sequences of MMIG-1. MMIG-1 comprises an N-terminal PYRIN domain, a central NBS domain, and C-terminal 9 LRRs, and is likely to be a mouse counterpart of human PYPAF1 or a closely related molecule. To our knowledge, this is the first demonstration that a PYPAF1-related molecule is expressed in mast cells. MMIG-1 is localized in the cytosol of mast cells, with enrichment in punctate structures. Moreover, we found that there are several spliced variants as to the LRR domain of MMIG-1/PYPAF1. Individual variants show different kinetics of induction in BMMC during coculture and thus may have distinct functions, even though their expression levels are lower than that of the full-length form.

The PYRIN domain belongs to the death domain-fold superfamily that also includes the caspase recruitment domain (CARD), death domain and death effector domain (*19*, *26*). Similar to other death domain-fold molecules, the PYRIN domain is assumed to mediate homotypic interactions between two PYRIN domain–containing proteins. The first protein in this family, pyrin, has a PYRIN domain at the N-terminus and has been proposed to function in inflammatory signaling in myeloid cells (*15*, *16*). Mutations of the *pyrin* gene confer susceptibility to familial Mediterranean fever (*15*, *16*). ASC and DEFCAP-L, each of which has a C-terminal CARD, induce apoptosis when overexpressed in cells (*17–21*). ASC forms aggregate in the cytoplasm, the appearance of which correlates with apoptosis (*20*, *21*). The PYRIN domain of pyrin interacts with that of DEFCAP-L and exerts a negative-regulatory effect on DEFCAP-L–induced signaling (*21*). NBS/LRR proteins Nod1 and Nod2 activate NF-κB by interacting with RICK, an upstream activator of the IκB kinase complex (*27*). The oligomerization of these NBS/LRR proteins as well as Apaf-1 is mediated by the NBS domain, and induces the proximity and activation of downstream effectors through CARD-CARD homophilic interactions. The NBS/LRR proteins are also found in plants as a class of disease-resistant genes, in which the LRRs are involved in the recognition of various microbial components. Nod1 and Nod2 may be mammalian counterparts of plant disease-resistant gene products that function as cytoplasmic receptors for pathogen components (*28*). Indeed, mutations of the LRRs of Nod2 have been implicated in two inflammatory diseases, Blau syndrome and Crohn disease (*29–31*).

Thus, given the fact that proteins having these domains (*i.e*. PYRIN, NBS and/or LRR domains) have been implicated in signal transduction leading to cell differentiation, inflammatory response and apoptosis, it is tempting to speculate that MMIG-1, a likely mouse PYPAF1 homolog, also plays a role in such critical biological events. The assembly of PYRIN domain-containing proteins through PYRIN-PYRIN interactions implies that MMIG-1/PYPAF1 may function in a manner analogous to other NBS/LRR family members and transmit upstream signals for the activation of downstream PYRIN proteins recruited to the signaling complex. Indeed, it was recently shown that human PYPAF1 binds to ASC *via* the PYRIN domain and that this interaction leads to augmented NF-κB activation (*13*) and procaspase-1 activation leading to IL-1β processing and secretion (*32*). Moreover, several PYPAF1-related proteins, which are composed of PYRIN, NBS and LRR domains and exhibit similar functions to PYPAF1, were recently identified (*32*, *33*).

Of particular interest, human PYPAF1 has been proposed to be a causal gene for familial cold urticaria, an autosomal-dominant systemic inflammatory disease characterized by intermittent episodes of rash, arthralgia, fever and conjunctivitis after generalized exposure to cold, for Muckle-Wells syndrome, an autosomal-dominant periodic fever syndrome often accompanied by sensorineural hearing loss (*12*), and for chronic infantile neurological cutaneous and articular syndrome (*34*). In these diseases, point mutations are found in exon 3, which encompasses the NBS domain, revealing the functional importance of this domain. Moreover, human chromosome 1q44, to which the *PYPAF1* gene has been mapped (*12*), has also been implicated in rheumatoid arthritis (*35*). Considering that mast cells may play a role in several symptoms of these inflammatory diseases, it may be reasonable to consider that PYPAF1 can affect mast cell differentiation and effector functions in some ways. Increased expression of PYPAF1 in mouse experimental atopic dermatitis also supports this notion. Thus, functional analysis of PYPAF1 in mast cells will help to clarify the mechanisms regulating inflammation as well as the biochemical basis for cold-sensitive phenotypes.

This work was supported by a Grant-in-Aid for Scientific Research from the Ministry of Education, Science, Culture and Technology of Japan and the Sankyo Foundation of Life Science.

REFERENCES

1. Galli, S.J., Tsai, M., and Lantz, C.S. (1999) The regulation of mast cell and basophil development by the *kit* ligand, SCF, and IL-3 in *Signal Transduction in Mast Cells and Basophils* (E. Razin and J. Rivera, eds.) pp. 11–30, Springer-Verlag, New York

2. Kitamura, Y., Morii, E., and Jippo, T. (1999) The c-*kit* receptor and the mi transcription factor: two important molecules for mast cell development in *Signal Transduction in Mast Cells and Basophils* (E. Razin and J. Rivera, eds.) pp. 31–38, Springer-Verlag, New York
3. Echtenacher, B., Mannel, D.N., and Huntler, L. (1996) Critical protective role of mast cells in a model of acute septic peritonitis. *Nature* **381**, 75–77
4. Maraviya, R., Ikeda, T., Ross, E., and Abraham, S.N. (1996) Mast cell modulation of neutrophil influx and bacterial clearance at sites of infection through TNFα. *Nature* **381**, 77–81
5. Wong, G.W., Friend, D.S., and Stevens, R.L. (1999) Mouse and rat models of mast cell development in *Signal Transduction in Mast Cells and Basophils* (E. Razin and J. Rivera, eds.) pp. 39–53, Springer-Verlag, New York
6. Friend, D.S., Ghildyal, N., Austen, K.F., Gurish, M.F., Matsumoto, R., and Stevens, R.L. (1996) Mast cells that reside at different locations in the jejunum of mice infected with *Trichinella spiralis* exhibit sequential changes in their granule ultrastructure and chymase phenotype. *J. Cell Biol.* **135**, 279–290
7. Levi-Schaffer, F., Austen, K.F., Gravallese, P.M., and Stevens, R.L. (1986) Coculture of interleukin 3-dependent mouse mast cells with fibroblasts results in a phenotypic change of the mast cells. *Proc. Natl Acad. Sci. USA* **83**, 6485–6488
8. Levi-Schaffer, F., Dayton, E.T., Austen, K.F., Hein, A., Caulfield, J.P., Gravallese, P.M., Liu, F.T., and Stevens, R.L. (1987) Mouse bone marrow-derived mast cells cocultured with fibroblasts: morphology and stimulation-induced release of histamine, leukotriene B4, leukotriene C4, and prostaglandin D_2. *J. Immunol.* **139**, 3431–3441
9. Rennick, D., Hunte, B., Holland, G., and Thompson-Snipes, L. (1995) Cofactors are essential for stem cell factor-dependent growth and maturation of mast cell progenitors: comparative effects of interleukin-3 (IL-3), IL-4, IL-10, and fibroblasts. *Blood* **85**, 57–65
10. Ogasawara, T., Murakami, M., Suzuki-Nishimura, T., Uchida, M.K., and Kudo, I. (1997) Mouse bone marrow-derived mast cells undergo exocytosis, prostanoid generation, and cytokine expression in response to G protein-activating polybasic compounds after coculture with fibroblasts in the presence of c-*kit* ligand. *J. Immunol.* **158**, 393–404
11. Taketomi, Y., Sugiki, T., Saito, T., Ishii, S., Hisada, M., Suzuki-Nishimura, T., Uchida, M.K., Moon, T.C., Chang, H.W., Natori, Y., Miyazawa, S., Kikuchi-Yanoshita, R., Murakami, M., and Kudo, I. (2003) Identification of NDRG1 as an early inducible gene during *in vitro* maturation of cultured mast cells. *Biochem. Biophys. Res. Commun.* **306**, 339–346
12. Hoffman, H.M., Mueller, J.L., Broide, D.H., Wanderer, A.A., and Kolodner, R.D. (2001) Mutation of a new gene encoding a putative pyrin-like protein causes familial cold autoinflammatory syndrome and Muckle-Wells syndrome. *Nat. Genet.* **29**, 301–305
13. Manji, G.A., Wang, L., Geddes, B.J., Brown, M., Merriam, S., Al-Garawi, A., Mak, S.M., Lora, J., Briskin, M., Jurman, M., Cao, J., DiStefano, P.S., and Bertin, J. (2002) PYPAF1, a PYRIN-containing Apaf1-like protein that assembles with ASC and regulates activation of NF-κB. *J. Biol. Chem.* **277**, 11570–11575
14. Nagai, H., Ueda, Y., Ochi, T., Hirano, Y., Tanaka, H., Inagaki, N., and Kawada, K. (2000) Different role of IL-4 in the onset of hapten-induced contact hypersensitivity in BALB/c and C57BL/6 mice. *Br. J. Pharmacol.* **129**, 299–306
15. Chae, J.J., Centola, M., Aksentijevich, I., Dutra, A., Tran, M., Wood, G., Nagaraju, K., Kingma, D.W., Liu, P.P., and Kastner, D.L. (2000). Isolation, genomic organization, and expression analysis of the mouse and rat homologs of MEFV, the gene for familial mediterranean fever. *Mamm. Genome* **11**, 428–435
16. Centola, M., Wood, G., Frucht, D.M., Galon, J., Aringer, M., Farrell, C., Kingma, D.W., Horwitz, M.E., Mansfield, E., Holland, S.M., O'Shea, J.J., Rosenberg, H.F., Malech, H.L., and Kastner, D.L. (2000) The gene for familial Mediterranean fever, MEFV, is expressed in early leukocyte development and is regulated in response to inflammatory mediators. *Blood* **95**, 3223–3231
17. Hlaing, T., Guo, R.F., Dilley, K.A., Loussia, J.M., Morrish, T.A., Shi, M.M., Vincenz, C., and Ward, P.A. (2001) Molecular cloning and characterization of DEFCAP-L and -S, two isoforms of a novel member of the mammalian Ced-4 family of apoptosis proteins. *J. Biol. Chem.* **276**, 9230–9238
18. Chu, Z.L., Pio, F., Xie, Z., Welsh, K., Krajewska, M., Krajewski, S., Godzik, A., and Reed, J.C. (2001) A novel enhancer of the Apaf1 apoptosome involved in cytochrome c-dependent caspase activation and apoptosis. *J. Biol. Chem.* **276**, 9239–9245
19. Martinon, F., Hofmann, K., and Tschopp, J. (2001) The pyrin domain: a possible member of the death domain-fold family implicated in apoptosis and inflammation. *Curr. Biol.* **11**, R118–120
20. Masumoto, J., Taniguchi, S., Ayukawa, K., Sarvotham, H., Kishino, T., Niikawa, N., Hidaka, E., Katsuyama, T., Higuchi, T., and Sagara, J. (1999) ASC, a novel 22-kDa protein, aggregates during apoptosis of human promyelocytic leukemia HL-60 cells. *J. Biol. Chem.* **274**, 33835–33838
21. Richards, N., Schaner, P., Diaz, A., Stuckey, J., Shelden, E., Wadhwa, A., and Gumucio, D.L. (2001) Interaction between pyrin and the apoptotic speck protein (ASC) modulates ASC-induced apoptosis. *J. Biol. Chem.* **276**, 39320–39329
22. Inohara, N., Koseki, T., del Peso, L., Hu, Y., Yee, C., Chen, S., Carrio, R., Merino, J., Liu, D., Ni, J., and Nunez, G. (1999) Nod1, an Apaf-1-like activator of caspase-9 and nuclear factor-κB. *J. Biol. Chem.* **274**, 14560–14567
23. Ogura, Y., Inohara, N., Benito, A., Chen, F.F., Yamaoka, S., and Nunez, G. (2001) Nod2, a Nod1/Apaf-1 family member that is restricted to monocytes and activates NF-κB. *J. Biol. Chem.* **276**, 4812–4818
24. Geddes, B.J., Wang, L., Huang, W.-J., Lavellee, M., Manji, G.A., Brown, M., Jurman, M., Cao, J., Morgenstern, J., Merriam, S., Glucksmann, M.A., DiStefano, P.S., and Bertin, J. (2001) Human CARD12 is a novel CED4/Apaf-1 family member that induces apotosis. *Biochem. Biophys. Res. Commun.* **284**, 77–82
25. Zou, H., Henzel, W.J., Liu, X., Lutschg, A., and Wang, X. (1997) Apaf-1, a human protein homologous to *C. elegans* CED-4, participates in cytochrome c-dependent activation of caspase-3. *Cell* **90**, 405–413
26. Aravind, L., Dixit, V.M., and Koonin, E.V. (2001) Apoptotic molecular machinery: vastly increased complexity in vertebrates revealed by genome comparisons. *Science* **291**, 1279–1284
27. Inohara, N., Koseki, T., Lin, J., del Peso, L., Lucas, P.C., Chen, F.F., Ogura, Y., and Nunez, G. (2000) An induced proximity model for NF-κB activation in the Nod1/RICK and RIP signaling pathways. *J. Biol. Chem.* **275**, 27823–27831
28. Inohara, N., Ogura, Y., Chen, F.F., Muto, A., and Nunez, G. (2001) Human Nod1 confers responsiveness to bacterial lipopolysaccharides. *J. Biol. Chem.* **276**, 2551–2554
29. Ogura, Y., Bonen, D.K., Inohara, N., Nicolae, D.L., Chen, F.F., Ramos, R., Britton, H., Moran, T., Karaliuskas, R., Duerr, R.H., Achkar, J.P., Brant, S.R., Bayless, T.M., Kirschner, B.S., Hanauer, S.B., Nunez, G., and Cho, J.H. (2001) A frameshift mutation in NOD2 associated with susceptibility to Crohn's disease. *Nature* **411**, 603–606
30. Hugot, J.P., Chamaillard, M., Zouali, H., Lesage, S., Cezard, J.P., Belaiche, J., Almer, S., Tysk, C., O'Morain, C.A., Gassull, M., Binder, V., Finkel, Y., Cortot, A., Modigliani, R., Laurent-Puig, P., Gower-Rousseau, C., Macry, J., Colombel, J.F., Sahbatou, M., and Thomas, G. (2001) Association of NOD2 leucine-rich repeat variants with susceptibility to Crohn's disease. *Nature* **411**, 599–603
31. Miceli-Richard, C., Lesage, S., Rybojad, M., Prieur, A.M., Manouvrier-Hanu, S., Hafner, R., Chamaillard, M., Zouali, H., Thomas, G., and Hugot, J.P. (2001) CARD15 mutations in Blau syndrome. *Nat. Genet.* **29**, 19–20
32. Wang, L., Manji, G.A., Grenier, J.M., Al-Garawi, A., Merriam, S., Lora, J.M., Geddes, B.J., Briskin, M., DiStefano, P.S., and

Bertin, J. (2002) PYPAF7, a novel PYRIN-containing Apaf-1-like protein that regulates activation of NF-κB and caspase-1-dependent cytokine processing. *J. Biol. Chem.* **277**, 29874–29880

33. Grenier, J.M., Wang, L., Manji, G.A., Huang, W.J., Al-Garawi, A., Kelly, R., Carson, A., Merriam, S., Lora, J.M., Briskin, M., DiStefano, P.S., and Bertin, J. (2002) Functional screening of five PYPAF family members identifies PYPAF5 as a novel regulator of NF-κB and caspase-1. *FEBS Lett.* **530**, 73–78
34. Feldmann, J., Prieur, A-M., Quartier, P., Berquin, P., Certain, S., Cortis, E., Teillac-Hamel, D., Fisher, A., and de Saint Basile, G. (2002) Chronic Infantile neurological cutaneous and articular syndrome is caused by mutations in *CIA*S1, a gene highly expressed in polymorphonuclear cells and chondrocytes. *Amer. J. Hum. Genet.* **71**, 198–203
35. Jawaheer, D., Seldin, M.F., Amos, C.I., Chen, W.V., Shigeta, R., Monteiro, J., Kern, M., Criswell, L.A., Albani, S., Nelson, J.L., Clegg, D.O., Pope, R., Schroeder, H.W., Bridges, S.L., Pisetsky, D.S., Ward, R., Kastner, D.L., Wilder, R.L., Pincus, T., Callahan, L.F., Flemming, D., Wener, M.H., and Gregersen, P.K. (2001) A genomewide screen in multiplex rheumatoid arthritis families suggests genetic overlap with other autoimmune diseases. *Amer. J. Hum. Genet.* **68**, 927–936